

Deep EM with Hierarchical Latent Label Modelling for Multi-Site Prostate Lesion Segmentation

Wen Yan^{1,*}, Yipei Wang¹, Shiqi Huang¹, Natasha Thorley², Mark Emberton²; Vasilis Stavrinos^{3,4}, Yipeng Hu¹, Dean Barratt¹

¹ UCL Hawkes Institute; Department of Medical Physics and Biomedical Engineering, University College London, Gower St, London WC1E 6BT, London, U.K.

² Division of Surgery and Interventional Science, University College London, 10 Pond St, London NW3 2PS, U.K.

³ Cancer Institute, Urology Department, UCL Hospital, University College London, 16-18 Westmoreland St, London W1G 8PH, U.K

⁴ Radiology Department, Imperial College Healthcare, The Bays, S Wharf Rd, London W2 1NY, U.K.
`wen-yan@ucl.ac.uk`

Abstract. Label variability is a major challenge for prostate lesion segmentation. In multi-site datasets, annotations often reflect centre-specific contouring protocols, causing segmentation networks to overfit to local styles and generalise poorly to unseen sites in inference. We treat each observed annotation as a noisy observation of an underlying latent “clean” lesion mask, and propose a hierarchical expectation–maximisation (HierEM) framework that alternates between: (i) inferring a voxel-wise posterior distribution over the latent mask, and (ii) training a CNN using this posterior as a soft target and estimate site-specific sensitivity and specificity under a hierarchical prior. This hierarchical prior decomposes label-quality into a global mean with site- and case-level deviations, reducing site-specific bias by penalising the likelihood term contributed only by site deviations. Experiments on three cohorts demonstrate that the proposed hierarchical EM framework enhances cross-site generalisation compared to state-of-the-art methods. For pooled datasets evaluation, per-site mean DSC ranges from 29.50% to 39.69% across datasets; for leave-one-site-out generalisation, it ranges from 27.91% to 32.67%, yielding statistically significant improvements over comparison methods ($p < 0.039$). The method also produces interpretable per-site latent label-quality estimates (e.g., sensitivity $\alpha \sim [31.5\%, 47.3\%]$ at specificity $\beta \approx 0.99$), supporting post-hoc analyses of cross-site annotation variability. These results indicate that explicitly modelling site-dependent annotation can improve cross-site generalisation. Code is available via <https://anonymous.4open.science/r/HierEM-F2D3/>.

Keywords: Lesion segmentation · Hierarchical latent label · EM.

1 Introduction

Multiparametric MRI (mpMRI), including T2-weighted (T2W), diffusion-weighted imaging (DWI), apparent diffusion coefficient (ADC) maps and contrast-enhanced (DCE) modalities, is widely used to assess suspected prostate cancer (PCa) [2]. Clinicians often contour lesions to guide treatment planning and follow-up. Automated deep-learning methods aim to reduce this workload, yet it faces a significantly high-variance ground truth challenge. This label variability is rooted in site-specific annotation protocols, the institutional style formed by local expert training and specific imaging protocols that influence how boundaries are perceived, which creates site-specific label bias. Inter-reader agreement for prostate lesion contours on mpMRI is only moderate, with reported Dice often around ~ 0.4 [5,8]. The current paradigm creates a critical bottleneck: segmentation networks easily overfit to the local contouring style of the training sites. When deployed to a new institution, the model generalises poorly, as single-site training achieves only 4%–28% Dice on a held-out site [10]. By contrast, testing on within-site achieves around $\sim 20\% \sim 60\%$ Dice [16,3,13,1] with different datasets. This gap can be alleviated via test-site finetuning or calibration. However, such methods often lead to test-site-biased accuracy assessments. They force the model to match the local “observed” labels, which are themselves imperfect and biased. A truly multi-site training set (more than 10 sites) is expensive to curate for individual tasks that require coordination in labelling. PI-CAI is an example study with such a diverse collection of reference standards, but restricted to a primarily patient-level classification [12]. In many real-world applications, further finetuning or calibration at deployment may not be feasible or practical. While cross-site performance gaps may also stem from both imaging differences and label variation, pre-processing can partially mitigate the former. In this study, we focus on the impact of label-level variation.

We propose a latent-label modelling approach to address cross-site annotation variability. Our model is inspired by the sensitivity/specificity formulation popularised by STAPLE [15]. STAPLE performs multi-annotator label fusion at inference time for a fixed image, jointly estimating each annotator’s sensitivity and specificity under conditional-independence assumptions. Our setting and goal differ. We do not fuse multiple labels for the same case, as typically only one annotation is observed per case. Instead, we treat each site’s annotation as a site-dependent noisy observation of an unobserved latent “clean” lesion mask during training. This yields a STAPLE-like observation model embedded within a segmentation-learning framework, where label variability is decomposed into three components: (1) global population factors capturing lesion characteristics shared across sites; (2) site-specific effects modelling systematic offsets due to local contouring and imaging protocols; and (3) case-level variability capturing intrinsic ambiguity (e.g., small or low-contrast lesions) that affects all annotators regardless of protocol. In summary, we use site-specific sensitivity/specificity to represent these hierarchical label-quality parameters.

Learning is performed with an EM procedure [6] that alternates between inferring the latent consensus mask and updating model parameters. In the E-step,

we compute a voxel-wise posterior over the latent consensus mask by combining the network’s image-based prior with the annotation likelihood under the current model. In the M-step, we update the UNet using this posterior as soft targets, and re-estimate the site-/case-level label-quality parameters by maximising their marginal likelihood under a hierarchical prior. Iterating these steps reduces dependence on any single centre’s contouring style, yields calibrated probabilistic predictions, and provides interpretable sens/spec estimates that summarise site tendencies and case-level ambiguity—improving robustness when deploying to unseen sites without requiring additional site-specific fine-tuning.

2 Method

Let Ω denote the voxel space of an mpMRI volume. For each case $k \in \{1, \dots, K\}$ we observe an image X_k and a single binary lesion annotation $Y_k \in \{0, 1\}^\Omega$ provided by one site $s_k \in \{1, \dots, S\}$. The (unobserved) latent “clean” lesion mask is $G_k \in \{0, 1\}^\Omega$. Our goal is to learn a segmentation model that is robust to site-specific annotation protocol, while also estimating site-/case-level latent label-quality parameters.

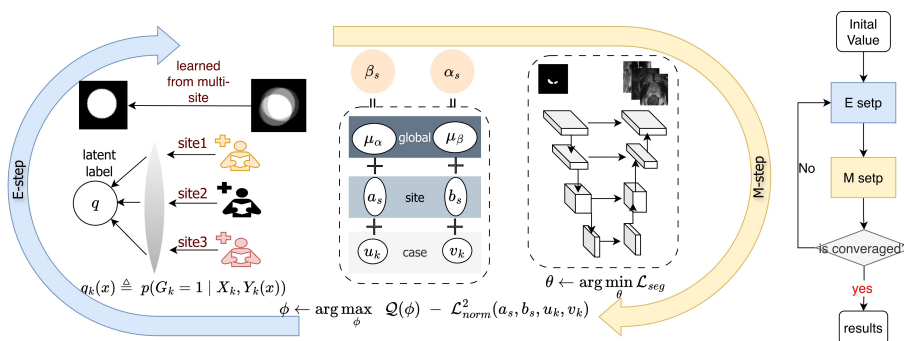


Fig. 1. Overview of proposed deep mixed EM framework with hierarchical latent label-quality parameters. The E-step infers a latent clean mask, and the M-step updates the segmentation network and latent label-quality parameters.

segmentation network We model the latent consensus mask with an image-conditioned voxel-wise probability map predicted by the network: $\pi_k(x) \triangleq p_\theta(G_k(x) = 1 | X_k) = \sigma(f_\theta(X_k)_x)$, where $x \in \Omega$ is a voxel in mpMRI, $f_\theta(\cdot)$ is a neural network producing logits per voxel and $\sigma(\cdot)$ is the sigmoid.

2.1 Hierarchical site-case label variability model

We treat each institute as a distinct annotation protocol and model the observed label $Y_k(x)$ as a noisy observation of $G_k(x)$. Conditioned on (G_k, s_k) , voxels are

assumed independent with site-case sensitivity and specificity:

$$p(Y_k(x) = 1 \mid G_k(x) = 1) = \alpha_{s_k, k}, \quad p(Y_k(x) = 0 \mid G_k(x) = 0) = \beta_{s_k, k}, \quad \forall x \in \Omega_k. \quad (1)$$

To stabilise site-/case-level label-quality estimates, we use a logistic-normal hierarchical prior that partially pools sens/spec toward a global mean μ_α, μ_β :

$$\text{logit}(\alpha_{s,k}) = \mu_\alpha + a_s + u_k, \quad \text{logit}(\beta_{s,k}) = \mu_\beta + b_s + v_k, \quad (2)$$

where (a_s, b_s) capture persistent site-specific contouring behavior and (u_k, v_k) capture case difficulty. We place zero-mean Gaussian priors (equivalently, ℓ_2 penalties under MAP): $a_s \sim \mathcal{N}(0, \sigma_a^2)$, $b_s \sim \mathcal{N}(0, \sigma_b^2)$, $u_k \sim \mathcal{N}(0, \sigma_u^2)$, $v_k \sim \mathcal{N}(0, \sigma_v^2)$. For identifiability we constrain $\sum_s a_s = 0$ and $\sum_s b_s = 0$. We further calculate site-level sen/spec as $(\sigma(\cdot))$ is sigmoid function):

$$\alpha_s = \sigma(\mu_\alpha + a_s), \quad \beta_s = \sigma(\mu_\beta + b_s) \quad (3)$$

EM learning with hierarchical sensitivity/specificity modelling We estimate segmentation network parameters θ and the latent label-quality parameters $\phi = \{\mu_\alpha, \mu_\beta, a_{1:S}, b_{1:S}, u_{1:K}, v_{1:K}\}$ by maximizing the (regularized) marginal likelihood of $\{Y_k\}$ with latent $\{G_k\}$. We optimise a MAP objective via an EM procedure.

E-step: posterior of the latent mask. Given current (θ, ϕ) , the posterior factorizes over voxels:

$$q_k(x) \triangleq p(G_k(x) = 1 \mid X_k, Y_k(x)) \quad (4)$$

$$= \frac{\pi_k(x) p(Y_k(x) \mid G_k(x) = 1)}{\pi_k(x) p(Y_k(x) \mid G_k(x) = 1) + (1 - \pi_k(x)) p(Y_k(x) \mid G_k(x) = 0)}. \quad (5)$$

With the sens/spec model, the likelihood terms are

$$p(Y=1 \mid G=1) = \alpha_{s,k}, \quad p(Y=1 \mid G=0) = 1 - \beta_{s,k}, \quad (6)$$

$$p(Y=0 \mid G=1) = 1 - \alpha_{s,k}, \quad p(Y=0 \mid G=0) = \beta_{s,k}. \quad (7)$$

$$p(Y|G; \alpha, \beta) = \begin{cases} \alpha^Y (1 - \alpha)^{1-Y}, & G = 1, \\ (1 - \beta)^Y \beta^{1-Y}, & G = 0. \end{cases} \quad (8)$$

Thus $q_k(x)$ provides a *soft consensus* mask that fuses the image prior and the site-case sens/spec.

M-step (A): update segmentation network. We update segmentation backbone with θ by minimising a soft-label cross-entropy plus Dice loss:

$$\mathcal{L}_{\text{seg}}(\theta) = \sum_{k=1}^K \sum_{x \in \Omega} \text{CE}(q_k(x), \pi_k(x)) - \sum_{k=1}^K \text{Dice}(q_k(x), \pi_k(x)), \quad (9)$$

where $\text{CE}(q, \pi) = -q \log \pi - (1-q) \log (1-\pi)$ and $\text{Dice}(q, \pi) = \frac{\sum_{x \in \Omega} 2q_k(x) \cdot \pi_k(x)}{\sum_{x \in \Omega} q_k(x) + \sum_{x \in \Omega} \pi_k(x)}$

M-step (B): update hierarchical latent label-quality by aggregated expected counts.
Define expected per-case sufficient statistics:

$$TP_k = \sum_{x \in \Omega} q_k(x) Y_k(x), \quad P_k = \sum_{x \in \Omega} q_k(x), \quad (10)$$

$$TN_k = \sum_{x \in \Omega} (1 - q_k(x)) (1 - Y_k(x)), \quad N_k = \sum_{x \in \Omega} (1 - q_k(x)). \quad (11)$$

Using posterior q to approximate latent Ground Truth G , the expected complete-data log-likelihood for latent label-quality parameters is:

$$\mathcal{Q}(\phi) = \mathbb{E}_{G \sim q} [\log p(Y|G; \phi)] \quad (12)$$

$$= \sum_{x \in \Omega} \left[\mathbb{1}\{G_k(x) = 1\} \left(Y_k(x) \log \alpha_{s_k, k} + (1 - Y_k(x)) \log (1 - \alpha_{s_k, k}) \right) \right. \\ \left. + \mathbb{1}\{G_k = 0\} \left((1 - Y_k(x)) \log \beta_{s_k, k} + Y_k(x) \log (1 - \beta_{s_k, k}) \right) \right] \quad (13)$$

$$= \sum_{k=1}^K \left[TP_k \log \alpha_{s_k, k} + (P_k - TP_k) \log(1 - \alpha_{s_k, k}) \right. \\ \left. + TN_k \log \beta_{s_k, k} + (N_k - TN_k) \log(1 - \beta_{s_k, k}) \right], \quad (14)$$

with $\alpha_{s, k}, \beta_{s, k}$ defined by (2). We obtain a MAP estimate by maximising MLE and L2 penalisation on prior variables in ϕ :

$$\phi \leftarrow \arg \max_{\phi} \mathcal{Q}(\phi) - \mathcal{L}_{norm}^2, \quad (15)$$

where $\mathcal{L}_{norm}^2 = \frac{1}{2\sigma_a^2} \sum_s a_s^2 + \frac{1}{2\sigma_b^2} \sum_s b_s^2 + \frac{1}{2\sigma_u^2} \sum_k u_k^2 + \frac{1}{2\sigma_v^2} \sum_k v_k^2$ subject to $\sum_s a_s = 0$ and $\sum_s b_s = 0$. Because (15) depends on the data only via (TP_k, P_k, TN_k, N_k) , it can be optimised efficiently with a few iterations of a second-order L-BFGS [7] over low-dimensional parameters. L_2 penalty on the hierarchical latent variables in ϕ corresponds to a Gaussian prior and provides shrinkage that stabilises site/case quality estimates, prevents degenerate sens/spec values, and mitigates overfitting when annotations are sparse or noisy.

Training procedure We alternate the E-step (5) with M-steps (9) and (15) until convergence. We used 10^{-4} learning-rate and Adam optimiser. In practice, we perform 5-epoch gradient steps for θ per EM iteration, and 5 optimiser steps for ϕ using the aggregated sufficient statistics in (14). Algorithm 1 summarises the procedure. To stabilise early optimisation, we add an auxiliary supervision in (9) using the ground-truth mask. The corresponding loss weight gradually decayed to zero over the first 5 epochs with a sigmoid ramping up strategy.

2.2 Uncertainty and interpretability

We quantify voxel-wise uncertainty using the predictive entropy of the segmentation probability map. The entropy at voxel i is $H_i = -p_i \log(p_i) - (1 -$

Algorithm 1 Hierarchical EM for multi-site lesion segmentation

Require: Images $\{X_k\}$, masks $\{Y_k\}$, site labels $\{s_k\}$

- 1: Initialize network parameters θ ; initialize ϕ (μ_α, μ_β near $\text{logit}(0.9)$, $a_s = b_s = u_k = v_k = 0$)
 - 2: **for** EM iterations $t = 1, \dots, T$ **do**
 - 3: **E-step:** compute $\pi_k(x) = \sigma(f_\theta(X_k)_x)$ and $q_k(x)$ via (5)
 - 4: Compute (TP_k, P_k, TN_k, N_k) via (10)–(11)
 - 5: **M-step (A):** update θ by minimizing $\mathcal{L}_{\text{seg}}(\theta)$ in (9)
 - 6: **M-step (B):** update ϕ by MAP optimization of (15) with constraints $\sum_s a_s = 0$, $\sum_s b_s = 0$
 - 7: **end for**
 - 8: **Output:** network θ and learned site-/case-level estimated parameters ϕ
-

$p_i) \log(1 - p_i)$. Entropy is small when p_i is close to 0 or 1 (confident predictions) and maximised at $p_i = 0.5$. To evaluate whether uncertainty aligns with segmentation errors, we construct a risk-coverage curve by ranking voxels by entropy and retaining the lowest-entropy fraction $c \in [0.5, 0.9]$. For each c , we choose a threshold t_c such that $S_c = \{i : H_i \leq t_c\}$, $\frac{|S_c|}{|\Omega|} = c$, where Ω denotes the set of all voxels. We then compute the Dice score restricted to the retained set S_c , denoted $\text{Dice}(S_c)$, and define risk as $\text{Risk}(c) = 1 - \text{Dice}(S_c)$.

3 Experiment

3.1 Datasets

We utilised datasets from $S = 3$ sites. Each site provides T2w, $\text{DWI}_{\text{high } b}$, and ADC images, together with a single expert lesion contour annotated on T2w. Sites 1 is acquired at the *anonymous institute*, comprising 1201 mpMR scans, each with $\text{PIRADS} \geq 3$ lesions. Site 2 is a public cohort [14], which includes 391 patients who have Likert ≥ 3 lesions. Site 3 is obtained from *anonymous institute*, containing 1265 mpMRI scans with $\text{PIRADS} \geq 3$ lesion contours.

Split A (Pooled mixture patient from multiple sites). We split each dataset by a 4:1:1 ratio, resulting in pooled mixed train, validation and per-patient level held-out sets. The held-out sets were only used for model evaluation.

Split B (Cross-site generalisation, LOSO). We perform leave-one-site-out evaluation across the 3 sites. For each fold, we hold out all cases from one site as test, and train on the remaining two sites. Within the training pool, we reserve 10% of cases (stratified by site) as validation for early stopping and hyperparameter tuning.

3.2 Baselines and evaluation metrics

Baselines In this study, to ensure a fair and transparent comparison across methods, we use UNet [11] with nnUNet-derived preprocessing and hyperparameters [4] as the segmentation backbone of the proposed and all other compared

Table 1. In the pooled patient-level held-out setting, Sites 1-3 include 252, 87, 265 cases in the patient-level held-out set, respectively; In the LOSO setting, Sites 1-3 include 1201, 391 and 1265 cases in the site-level held-out set, respectively. * denote HierEM is significantly better than other baselines $p < 0.05$.

Methods	Site 1		Site 2		Site 3	
	Dice(%)	HD95(mm)	Dice(%)	HD95(mm)	Dice(%)	HD95(mm)
<i>Split A: Pooled patient-level held-out split</i>						
UNet	38.63±10.41	17.04±2.96	27.47±9.62*	21.25±4.50	33.49±6.98*	22.06±3.92
Bootstrap	38.49±9.94	16.97±3.14	26.69±10.59*	22.29±5.12*	33.14±7.05*	21.41±5.84
Site-EM	36.46±11.72*	18.41±7.07*	23.74±9.73*	22.99±5.52*	34.62±6.15	21.86±4.91
HierEM	39.69±21.88	16.92±3.29	29.50±9.13	20.46±5.58	35.60±7.85	21.66±4.11
<i>Split B: Leave-one-site-out (LOSO)</i>						
UNet	25.50±7.33*	22.10±4.65*	24.66±5.29*	22.46±3.15*	31.20±9.80*	21.05±5.64
Bootstrap	26.34±12.92*	21.02±7.02*	21.66±5.20*	22.54±3.56*	31.64±8.92*	22.85±5.17
Site-EM	24.00±18.09*	23.74±10.79*	24.92±13.29*	21.83±7.13	31.90±13.43*	22.50±7.28
HierEM	28.11±10.21	20.51±4.68	27.91±10.16	21.12±5.83	32.67±8.08	22.82±2.50

methods. We compare against: (i) UNet only; (ii) Label bootstrapping (soft self-training) [9]: We replaced the standard supervised loss with a bootstrapped self-training loss that combines the provided labels with the model’s own predictions as soft auxiliary targets: $\mathcal{L}_{bootstrap}^{t+1} = (1-\lambda)\mathcal{L}_{seg}(\omega^{t+1}, y) + \lambda\mathcal{L}_{seg}(\omega^{t+1}, \omega^t)$, where ω^t is the network prediction at t iteration and λ is ramping up hyperparameter (max: 0.5). This encourages smoother decision boundaries and reduces sensitivity to annotation noise. (iii) Site-as-reader EM without hierarchy (independent α_s, β_s per site rather than using (2)).

Evaluation metrics for segmentation and uncertainty On each test fold and site, we report Dice and HD95 for segmentation results. For calibration and uncertainty metrics, we report selective segmentation (risk-coverage) curves based on predicted uncertainty (entropy of $q_k(x)$). We compare methods using a paired t -test on the same test cases within each held-out site. Multiple comparisons are controlled within each held-out site using Benjamini-Hochberg FDR at 5%.

4 Results

Table 1 reports cross-site performance using Dice and HD95. Under the pooled patient-level held-out split, all methods achieve moderate Dice (\sim 27–40) while HierEM gives the best mean Dice on all three sites (Site 1: 39.69%, Site 2: 29.50%, Site 3: 35.60%) and comparable or slightly improved HD95 (e.g., Site 2: 20.46 vs 21.25 for Supervised). Bootstrap is broadly similar to Supervised on the pooled split. In the pooled held-out split, significance is not observed for every comparison, likely due to limited test-set size. In addition, pooled multi-site training improves baseline performance, so our method shows a smaller

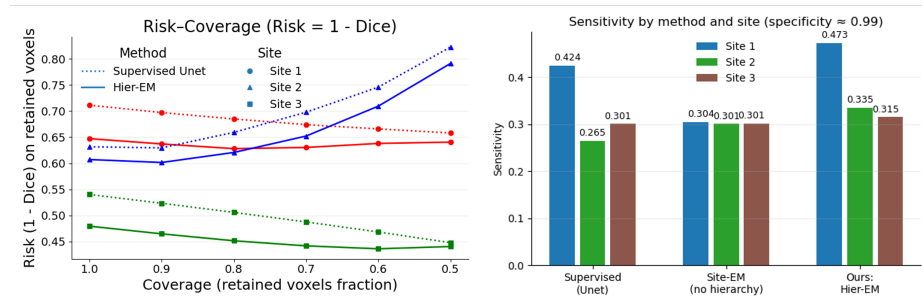


Fig. 2. Left: Risk-coverage curves on three sites dataset under LOSO experiments; Right: Estimated sensitivity of baselines and HierEM with $spec \simeq 0.99$. Such high specificity is expected because lesions occupy only a small fraction of the image.

margin in this setting. Under the more challenging LOSO evaluation, performance drops substantially for methods trained without explicit cross-site label variability modelling. Supervised Dice decreases to 25.50/24.66/33.09% across Sites 1–3, with a concurrent increase in boundary error (HD95 22–24 mm). In contrast, HierEM consistently improves generalisation, yielding higher Dice on Sites 1 and 2 (28.11 and 27.40 mm) with lower HD95 (20.51 and 20.31 mm), while remaining competitive on Site 3 (Dice 32.67%; HD95 22.82 mm). Overall, HierEM provides the most consistent cross-site performance, especially in the LOSO setting. Fig 2-left shows risk–coverage curves that assess uncertainty for selective segmentation. HierEM has lower risks than supervised UNet at a given coverage range for all three sites LOSO experiments, which indicates that the method’s uncertainty concentrates errors in the rejected region, enabling reliable abstention. In Figure 2-right, the HierEM achieved the highest sensitivity under the matched specificity ($\simeq 0.99$) on all LOSO experiments. Since lesions occupy a small fraction of voxels, operating at high specificity is reasonable.

The gap between pooled and LOSO highlights a strong domain shift: models that perform reasonable on pooled held-out testing degrade when the test site is unseen, suggesting that performance in pooled splits largely comes from learning site-specific contouring biases rather than fully transferable latent “clean” lesion mask. HierEM narrows this gap, supporting the hypothesis that explicitly modelling site/case-dependent label noise helps separate site-specific annotation from image evidence. By inferring a soft latent consensus mask(q) and updating sens/spec, HierEM reduces the overfitting when moving to a new centre, which is reflected in both higher Dice and lower HD95 on unseen sites.

5 Conclusion

We present a Deep EM framework that treats each site’s lesion contour as a noisy observation of an underlying latent “clean” mask. The E-step aggregates site annotations into a voxel-wise posterior over the latent mask; the M-step updates the

network while jointly estimating site-specific sensitivity and specificity with hierarchical shrinkage to stabilise quality estimates under limited sites of data. This formulation disentangles latent label from site-dependent contouring style, improving robustness and generalisation in cross-site evaluation. Beyond accuracy gains, it provides interpretable, site-level diagnostics of annotation behaviour that can guide data curation and deployment. HierEM is compatible with different backbone networks. Future work will extend the framework to multi-site, multi-annotator datasets and explore richer annotation-variability models in real clinical workflows.

Acknowledgments. This work is supported by the International Alliance for Cancer Early Detection, an alliance between Cancer Research UK [C28070/A30912; C73666/A31378; EDDAMC-2021/100011], Canary Center at Stanford University, the University of Cambridge, OHSU Knight Cancer Institute, University College London and the University of Manchester. This work is also supported by the National Institute for Health Research (NIHR) University College London Hospitals (UCLH) Biomedical Research Centre (BRC).

References

1. Fouladi, S., Darvizeh, F., Gianini, G., Di Meo, R., Di Palma, L., Damiani, E., Maiocchi, A., Fazzini, D., Ali, M.: Exploring unet-based models for prostate lesion segmentation from multi-sequence mri (t2w, adc, dwi). *World Wide Web* **29**(1), 4 (2026)
2. Haider, M.A., Van Der Kwast, T.H., Tanguay, J., Evans, A.J., Hashmi, A.T., Lockwood, G., Trachtenberg, J.: Combined t2-weighted and diffusion-weighted mri for localization of prostate cancer. *American journal of roentgenology* **189**(2), 323–328 (2007)
3. Hambarde, P., Talbar, S., Mahajan, A., Chavan, S., Thakur, M., Sable, N.: Prostate lesion segmentation in mr images using radiomics based deeply supervised u-net. *Biocybernetics and Biomedical Engineering* **40**(4), 1421–1435 (2020)
4. Isensee, F., Jaeger, P.F., Kohl, S.A., Petersen, J., Maier-Hein, K.H.: nnu-net: a self-configuring method for deep learning-based biomedical image segmentation. *Nature methods* **18**(2), 203–211 (2021)
5. Liechti, M.R., Muehlethaler, U.J., Schneider, A.F., Eberli, D., Rupp, N.J., Hötter, A.M., Donati, O.F., Becker, A.S.: Manual prostate cancer segmentation in mri: interreader agreement and volumetric correlation with transperineal template core needle biopsy. *European radiology* **30**(9), 4806–4815 (2020)
6. Moon, T.K.: The expectation-maximization algorithm. *IEEE Signal processing magazine* **13**(6), 47–60 (1996)
7. Nocedal, J.: Updating quasi-newton matrices with limited storage. *Mathematics of computation* **35**(151), 773–782 (1980)
8. Piert, M., Shankar, P.R., Montgomery, J., Kunju, L.P., Rogers, V., Siddiqui, J., Rajendiran, T., Hearn, J., George, A., Shao, X., et al.: Accuracy of tumor segmentation from multi-parametric prostate mri and 18f-choline pet/ct for focal prostate cancer therapy applications. *EJNMMI research* **8**(1), 23 (2018)

9. Reed, S., Lee, H., Anguelov, D., Szegedy, C., Erhan, D., Rabinovich, A.: Training deep neural networks on noisy labels with bootstrapping. arXiv preprint arXiv:1412.6596 (2014)
10. Rodrigues, N.M., de Almeida, J.G., Castro Verde, A.S., Mascarenhas Gaivão, A., Bilreiro, C., Santiago, I., Ip, J., Belião, S., Moreno, R., Matos, C., Vanneschi, L., Tsiknakis, M., Marias, K., Regge, D., Silva, S., Papanikolaou, N., ProCancer-I Consortium: Analysis of domain shift in whole prostate gland, zonal and lesions segmentation and detection, using multicentric retrospective data. *Computers in Biology and Medicine* p. 108216 (2024). <https://doi.org/10.1016/j.compbimed.2024.108216>
11. Ronneberger, O., Fischer, P., Brox, T.: U-net: Convolutional networks for biomedical image segmentation. In: *International Conference on Medical image computing and computer-assisted intervention*. pp. 234–241. Springer (2015)
12. Saha, A., Bosma, J., Twilt, J., van Ginneken, B., Yakar, D., Elschot, M., Veltman, J., Fütterer, J., de Rooij, M., et al.: Artificial intelligence and radiologists at prostate cancer detection in mri—the pi-cai challenge. In: *Medical Imaging with Deep Learning, short paper track* (2023)
13. Wang, W., Pan, B., Ai, Y., Li, G., Fu, Y., Liu, Y.: Paracm-pnet: A cnn-tokenized mlp combined parallel dual pyramid network for prostate and prostate cancer segmentation in mri. *Computers in Biology and Medicine* **170**, 107999 (2024)
14. Wang, Y., Gayo, I., Thorley, N., Ng, A., Yan, W., Barratt, D., Stavrinides, V., Emberton, M., Kasivisvanathan, V., Punwani, S., Hu, Y.: A derived promis data set (Jun 2025). <https://doi.org/10.5281/zenodo.15683922>, <https://doi.org/10.5281/zenodo.15683922>
15. Warfield, S.K., Zou, K.H., Wells, W.M.: Simultaneous truth and performance level estimation (staple): an algorithm for the validation of image segmentation. *IEEE transactions on medical imaging* **23**(7), 903–921 (2004)
16. Yan, W., Hu, Y., Yang, Q., Fu, Y., Syer, T., Min, Z., Punwani, S., Emberton, M., Barratt, D.C., Cho, C.C., et al.: A semi-supervised prototypical network for prostate lesion segmentation from multimodality mri. *Physics in Medicine & Biology* **70**(8), 085020 (2025)